Quaternary Stratigraphic Division and Paleoenvironmental Evolution Observed from Core LZK1 on Hengsha Island, Shanghai

KE Xue[1, 2, *], XIE Jianlei[3], ZHANG Zongyan[4], ZOU Yarui[5] and WANG Guoquan[6]

[1] *Institute of Geological Survey, China University of Geosciences, Wuhan 430074, China*
[2] *State Key Laboratory of Biogeology and Environmental Geology, China University of Geosciences, Wuhan 430074, China*
[3] *Shanghai Institute of Geological Survey, Shanghai 200072, China*
[4] *Wuhan Center, China Geological Survey, Wuhan 430205, China*
[5] *Hubei Institute of Geosciences, Wuhan 430034, China*
[6] *Department of Earth and Atmospheric Sciences, University of Houston, Houston, TX 77204, USA*

Abstract: The Quaternary sediments in the Yangtze delta are loose and lack precise stratification marks in the lithology. Moreover, due to the limitations of dating methods, it is difficult for Quaternary cores to deliver accurate age constraints. Thus, it is a challenge to establish the Quaternary stratigraphic framework. Gravity core LZK1 was drilled on Hengsha Island, Shanghai, in the Yangtze delta, in 2012. The core was terminated at 403.83 m below the local land surface, the uppermost 291.2 m comprising a thick sequence of Quaternary sediments. This study investigated the stratigraphic subdivision and paleoenvironmental change of the Quaternary sediments. From bottom to top, the Quaternary stratigraphic sequence can be subdivided into the lower Pleistocene Anting Formation, Middle Pleistocene Jiading Formation, Upper Pleistocene Chuansha Formation and Nanhui Formation, Holocene Loutang Formation, Shanghai Formation, and Rudong Formation. According to this study, the Hengsha Island area was dominated by a freshwater lacustrine environment during the early Pleistocene, an alternation of shallow lake and shore lake environment during the Middle Pleistocene, a delta plain to lagoonal environment during the early Upper Pleistocene, a fluvial channel to floodplain environment from the LGM (Last Glacial Maximum) to the end of the Upper Pleistocene, and a delta environment during the Holocene.

Key words: chronostratigraphic framework, paleoenvironmental evolution, marine transgression, Quaternary, Yangtze delta

Citation: Ke et al., 2020. Quaternary Stratigraphic Division and Paleoenvironmental Evolution Observed from Core LZK1 on Hengsha Island, Shanghai. Acta Geologica Sinica (English Edition), 94(4): 1167–1177. DOI: 10.1111/1755-6724.14564

1 Introduction

In recent years, Quaternary environmental change and its relationship to climate change, sea-level fluctuation and human activities in the Yangtze delta area have frequently been investigated (e.g., Han and Yu, 2001; Liu et al., 2010; Duan et al., 2016; Wang et al., 2010, 2011; Zhang et al., 2017; Cheng et al., 2019). The main part of the Yangtze delta is the incised paleo-valley, which is bounded by the Yizheng-Yangzhou-Hai'an in the north and the Zhenjiang-Jiangyin-Zhangjiagang and the south bank of the Yangtze River to the south (Fig. 1; Li et al., 2000, 2002). Due to the loose Quaternary sediments in the Yangtze delta, the marks of the lithostratigraphic subdivision are not clear. Furthermore, the lack of a well-dated core makes it difficult to establish the Quaternary geochronological framework. In order to further explore Quaternary environmental evolution, a regional chronostratigraphic framework needs to be established. Gravity core LZK1 was drilled on Hengsha Island, Shanghai, for geological survey purposes (Xie, 2017). The core is located in the incised Yangtze paleo-valley and the present-day Yangtze estuary. The Quaternary deposits were influenced by both river and ocean sedimentary systems. The details of the depositional environments within the Yangtze paleo-valley and estuary were not clear at the time that this investigation was conducted. This study aims to investigate the change of sedimentary environments during the Quaternary in the Yangtze delta region, which is fundamental to understanding regional sedimentary cycles and paleoenvironmental evolution.

* Corresponding author. E-mail: xue_ke@cug.edu.cn

2 Geological Settings

2.1 Regional geological settings

The regional tectonic unit of the Shanghai area belongs to the southern margin of the Yangtze block (Guo et al., 1997). The eastern subsidence zone has been developing continuously since the uplift of the Qinghai-Tibetan Plateau caused by the Quaternary neotectonic orogeny (Wang et al., 2008). The Shanghai area subsided from the land region in the southwest to the estuary region in the northeast in sequence, forming a late Cenozoic sedimentary basin with the characteristics of uplift in the southwest and subsidence in the northeast (Qiu and Li, 2007). This sedimentary basin is mainly covered by the thick loose sediments of the late Cenozoic. The paleoenvironmental change of the Shanghai area is associated with both the development of the Yangtze delta and some historical fragments of the East China sea (Chen and Stanley, 1995; Wang et al., 2004).

The Quaternary strata in the Shanghai area are well-developed and widely distributed. The distribution of the Quaternary sediments in the delta area was controlled by the sea-level fluctuation associated with tectonic movements, supply of sediments, and paleoclimatic changes (Huang et al. 2019). Tectonic movements and climate changes also resulted in the differences in lithology, lithofacies and the thickness of the strata (Jiang et al., 2000). The Quaternary stratigraphic sequence of the Shanghai area is 200–350 m thick (Wu and Li, 1987; Chen and Stanley, 1995), consisting of the Anting Formation (lower Pleistocene), Jiading Formation (Middle Pleistocene), Chuansha Formation (Upper Pleistocene), Nanhui Formation (Upper Pleistocene), Loutang Formation (lower Holocene), Shanghai Formation (middle Holocene) and Rudong Formation (upper Holocene). The discordant surface or discontinuous depositional surface is often used as a marker among the units to reflect the emergence of new depositional cycles (Qiu et al., 2006).

2.2 Core description

Core LZK1 was drilled on Hengsha Island, Shanghai (31°20′N, 121°50′E; Fig. 1). The elevation of the land surface at the core site is 0.25 m above sea level as defined by the China National Vertical Datum (CNVE, 1985). The core was recovered using a rotary drilling system with a diameter of 108 mm. The drilling depth was 408.83 m. The recovery rate of the core was approximately 90%. The Quaternary sediment ended at 219.2 m below the surface (Xie et al., 2017). The top half meter (0–0.6m) of the core is plain fill, but the portion below 0.6 m can be divided into the following nine units according to composition, color, and sedimentary grain size (Fig. 2).

Unit 1 (0.6–12.0 m) consists of alternating gray silty clay and silt, with both horizontal and microwave bedding. Iron and manganese spots and humus layers can occasionally be observed. Unit 2 (12.0–33.7 m) consists of gray clay, intercalated with thin layers of silt and clayey silt. The silt layers contain shells and shell debris, with lenticular bedding, horizontal bedding, and convolute bedding in some parts. Unit 3 (33.7–46.1 m) consists of taupe or grayish-yellow silt and silty clay in the lower part, with a high content of organic matter, occasional roots of plants and shell debris, with horizontal bedding. The upper part consists of alternating gray-taupe clay and silt or clayey silt, with lenticular, horizontal and convolute bedding. Unit 4 (46.1–87.3 m) mainly consists of yellowish-gray coarse sand with gravel, medium-fine sand, silty fine sand. The lower part consists of more subangular or subcircular gravels with diameters ranging from 2 to 5 mm. The grain size shows a fining-upward trend. Some parts contain interbedded clayey silt and silt, with horizontal, wavy and flaser bedding. Unit 5 (87.3–112.0 m) consists of gray medium-fine sand in the bottom, subangular or subcircular gravels in some parts with diameters spanning 2–3 mm, overlain by gray plastic clay, with a high content of organic matter in some parts, with horizontal and wavy bedding. Unit 6 (112.0–143.0 m) consists of grayish-yellow silty fine sand with parallel bedding, overlain by silt or clayey silt-clay sedimentary

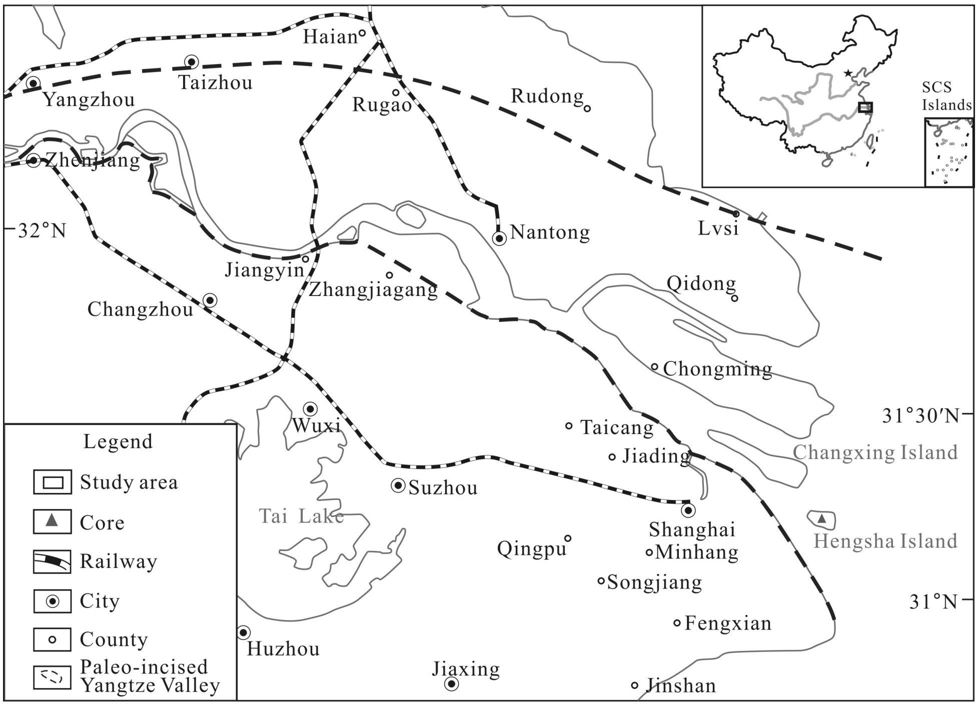

Fig. 1. Map showing the locations of core LZK1 and the paleo-incised Yangtze Valley. The boundary of the paleo-incised Yangtze Valley is modified from Li et al., 2000. SCS: South China Sea.

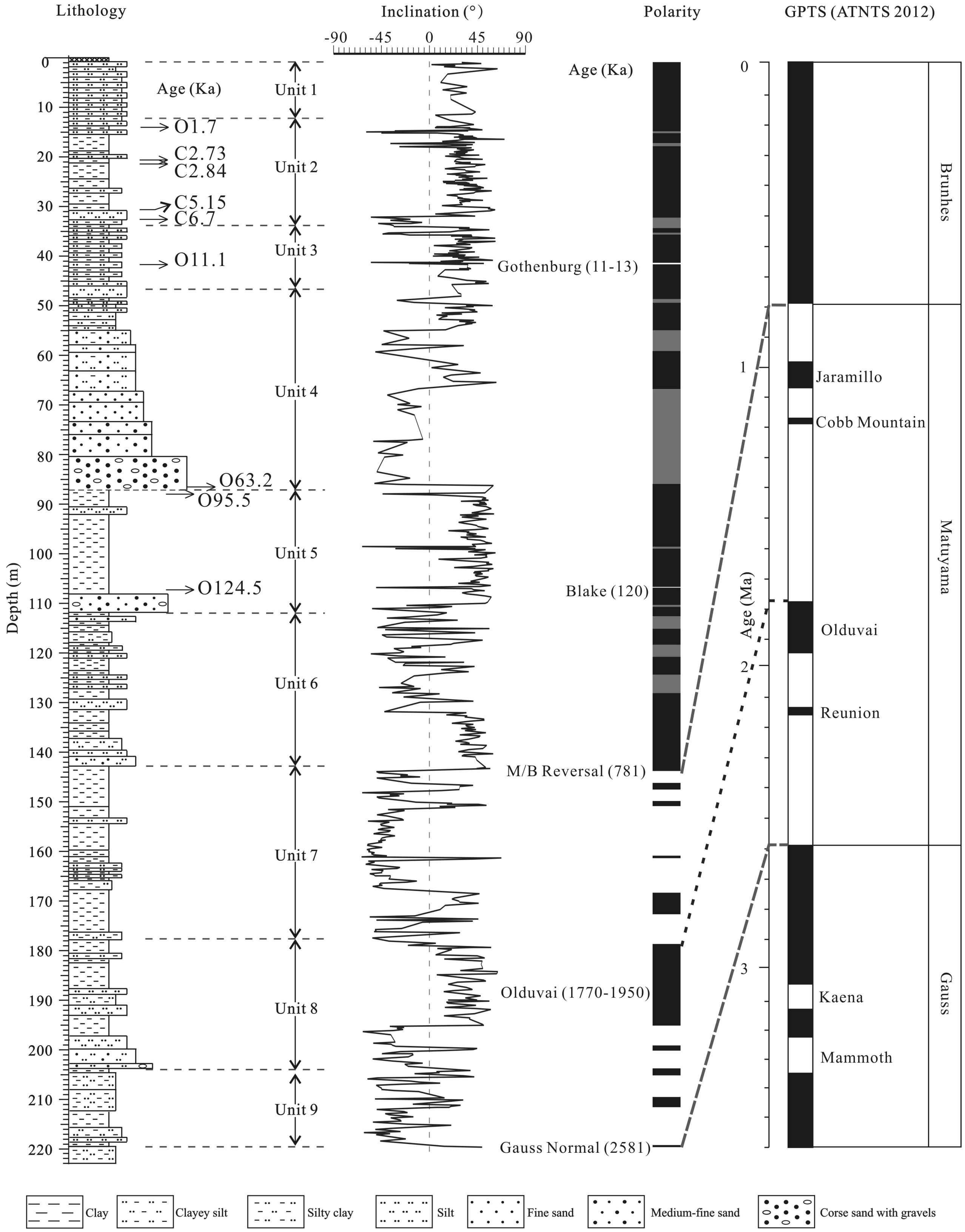

Fig. 2. Lithology and magnetostratigraphy of core LZK1 (modified from Xie et al., 2017) compared with the Geomagnetic Polarity Timescale (GPTS, ATNTS 2012) (Hilgen et al., 2012) and Geomagnetic Instability Time Scale (GITS) (Singer, 2014). Unit 1 to Unit 9 are depositional units.

cycles with lenticular and horizontal bedding. The middle and upper parts are composed of alternating silt and silty clay. These sedimentary cycles are gray or grayish-yellow in color, containing abundant white shell debris. The iron and manganese spots and calcareous concretions are observed in this unit. Unit 7 (143.0–178.0 m) consists of grayish-yellow or bluish-gray clay, intercalated with thin layers of clayey silt or silty clay, containing clay interbedded with clayey silt in some parts, with horizontal bedding. Unit 8 (178.0–204.6 m) consists of grayish-yellow coarse sand and silty fine sand with gravel in the bottom, overlain by four silt-silty clay-clay sedimentary cycles, containing iron and manganese spots, calcareous bands and concretions. The gravel is angular in shape, poorly sorted, with parallel bedding in some parts. Unit 9 (204.6–219.2 m) consists of grayish-yellow or blueish-gray silt, silty clay, and clay, containing iron and manganese spots, calcareous bands, and concretions.

3 Materials and Methods

In this study, a total of 1,085 oriented samples were collected across the section ranging from 0.6 to 219.2 m of core LZK1 for paleomagnetic analysis. As the core was obtained using a rotary drilling system, the horizontal orientation of the samples is arbitrary and has no geological meaning. The sampling interval was between 0.1 and 0.2 m for clayey silt and silt layers, and 0.5 m for sand layers. All the paleomagnetic samples were cut into cubes with dimensions of 2 × 2 × 2 cm. The paleomagnetic measurements were performed at the Paleomagnetism and Geochronology Laboratory of the Institute of Earth Environment, Chinese Academy of Sciences, Xi'an, China. A total of 1,085 samples were subjected to progressive alternating demagnetization in a 2G-600 alternating demagnetizer. Alternating demagnetization up to 80 mT included a maximum of 16 steps with intervals of 2.5–5 mT below 10 mT and 5–10 mT above. Remanence measurements were performed using a 2G-755R U-Channel cryogenic magnetometer housed in a magnetically- shielded room (background field < 300 nT). The magnetostratigraphy of the core was reported extensively in Xie et al. (2017).

AMS ^{14}C dates were obtained on shells from four samples by Beta Analytic Inc., Miami, Florida, USA (Xie et al., 2017). Eight samples of silt, fine sand or clayey silt around the boundaries of the different lithological units were collected from over the depth 0.6–110 m in core LZK1 for OSL dating, at the Groundwater Mineral Water and Environmental Monitoring Center, Ministry of Natural Resources, Shijiazhuang, China, using a Daybreak 2200 TL/OSL reader (Xie et al., 2017). Table 1 and Table 2 list the AMS ^{14}C dating results and OSL dating results, respectively.

A total of 998 samples for grain analyses were collected from throughout the core section 0.6–219.2 m at intervals of 20 cm. The grain analyses were performed at the State Key Laboratory of Biogeology and Environmental Geology at the China University of Geosciences, Wuhan, China and State Key Laboratory of Estuarine and Coastal Research at East China Normal University, Shanghai, China, using the Coulter LS230 and LS13320 LPSA (Laser Particle Size Analyzer), respectively. The parameters of grain size, including mean (M_z), skewness (SK_i), kurtosis (K_g), and standard deviation (σ_i), were calculated according to the method introduced in Folk and Ward (1957).

For microfossil (benthic foraminifers and ostracods) identification, 320 samples were analyzed from section 0.6 to 219.2 m with intervals of 20 cm. Micropaleontological analysis of the samples was conducted using the treatment method introduced by Ke et al. (2017) and the >74 μm fraction was examined under a stereoscopic microscope for foraminifers and ostracods. The abundances (numbers of individuals) and simple diversity (number of species) of the foraminifers and ostracods were calculated based on a dry sample of 50 g. The Shannon Index (Hs) was estimated to assess the variation of benthic foraminiferal complex diversity (Shannon, 1948).

4 Results

Foraminiferal specimens were found within sections of 0.6–46.1m and 87.4–92.0 m (Fig. 3). Most of the foraminifers were benthic forms, with planktonic types constituting less than 5%. 113 species of benthic foraminifers in 53 genera have been identified. In core LZK1, the abundance of the benthic foraminifers varies from 1 to 2285 specimens per 50 g of core sample. The simple diversity trend of benthic foraminiferal species is much like the trend of H(s), varying from 1–46 (Fig. 3). Most of the benthic foraminifers are hyaline tests. The porcellaneous forms are frequently observed in Unit 2, and arenaceous forms are occasionally observed. The dominant species in the core is *Ammonia beccarii* var., which approaches 50% on average. Other species, such as *Cribrononion subincertum*, *Elphidium advenum*, *Elphidium magellanicum* and *Florilus decoru*s are also frequently observed (Fig. 3).

Ostracod specimens were found within sections of 0.6–46.1 m and 105.9–163.0 m (Fig. 4). In total, 30 species (including 2 undetermined species) in 37 genera have been identified. The abundance of the ostracods varies from 1 to 450 specimens per 50 g. The simple diversity trend of ostracod species is the same as the trend of H(s), varying from 1–20 (Fig. 4). The dominant genera and species in the core LZK1 are *Sinocytheridea impressa*, *Albileberis sinesis*, *Bicornucythere bisanensis*, *Neomonoceratina dongtaiensis*, *Ilyocypris* spp., and *Candoniella* l spp. (Fig. 4). Other species, such as *Tanella opima Chen*, *Aurila cymba*, *Pistcythereis bradyformis* and *Pistcythereis bradyi* were also identified at a relatively high frequency.

The grain-size analysis of the Quaternary sediments includes mean (M_z), skewness (SK_i), kurtosis (K_g), and standard deviation (σ_i). Each parameter is important for evaluating the hydrodynamic conditions of sediment transport (Folk, 1966). In the core LZK1, these parameters show a remarkable correspondence with each other in the vertical direction (Fig. 5). The value of M_z varies within a broad range from −0.54 to 8.33Φ, which suggests that the source of supply or depositional environment has changed

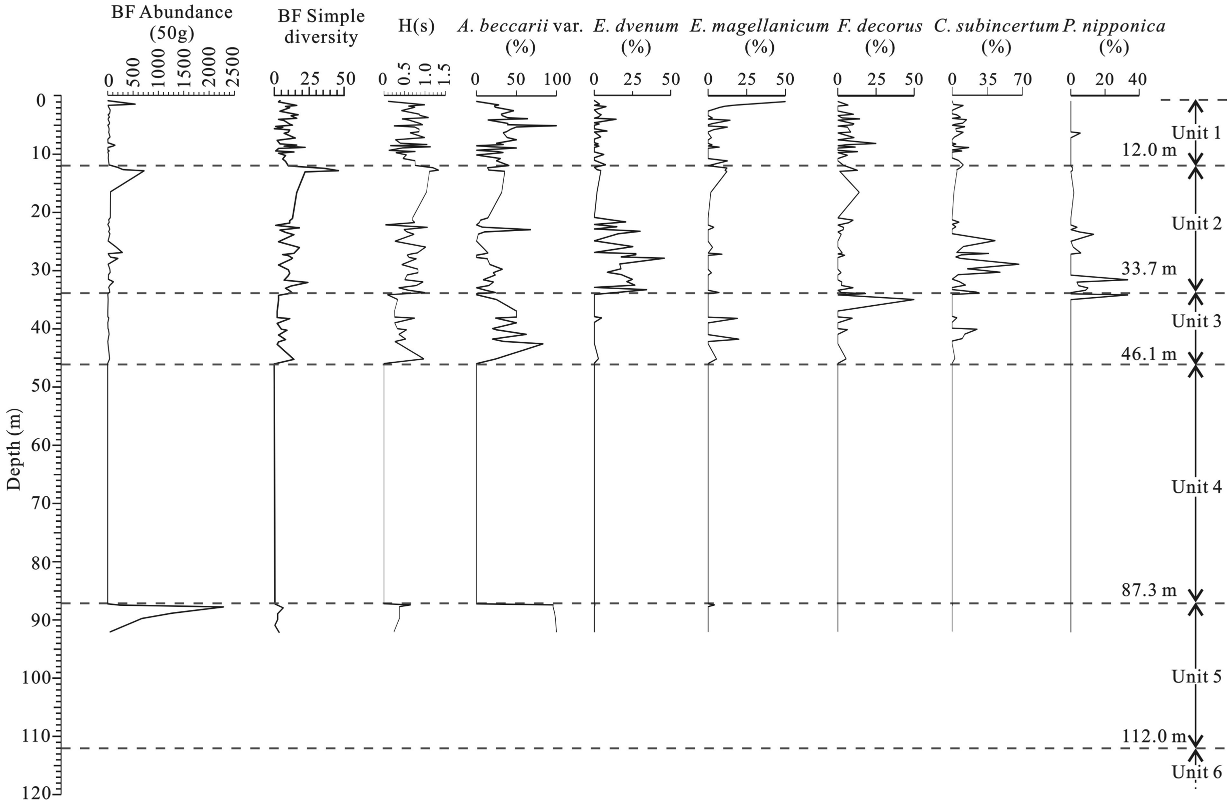

Fig. 3. Downcore changes in foraminiferal abundance, simple diversity, and Shannon index (H(s)), and the relative abundance of the main foraminiferal species in the uppermost 120 m of core LZK1.

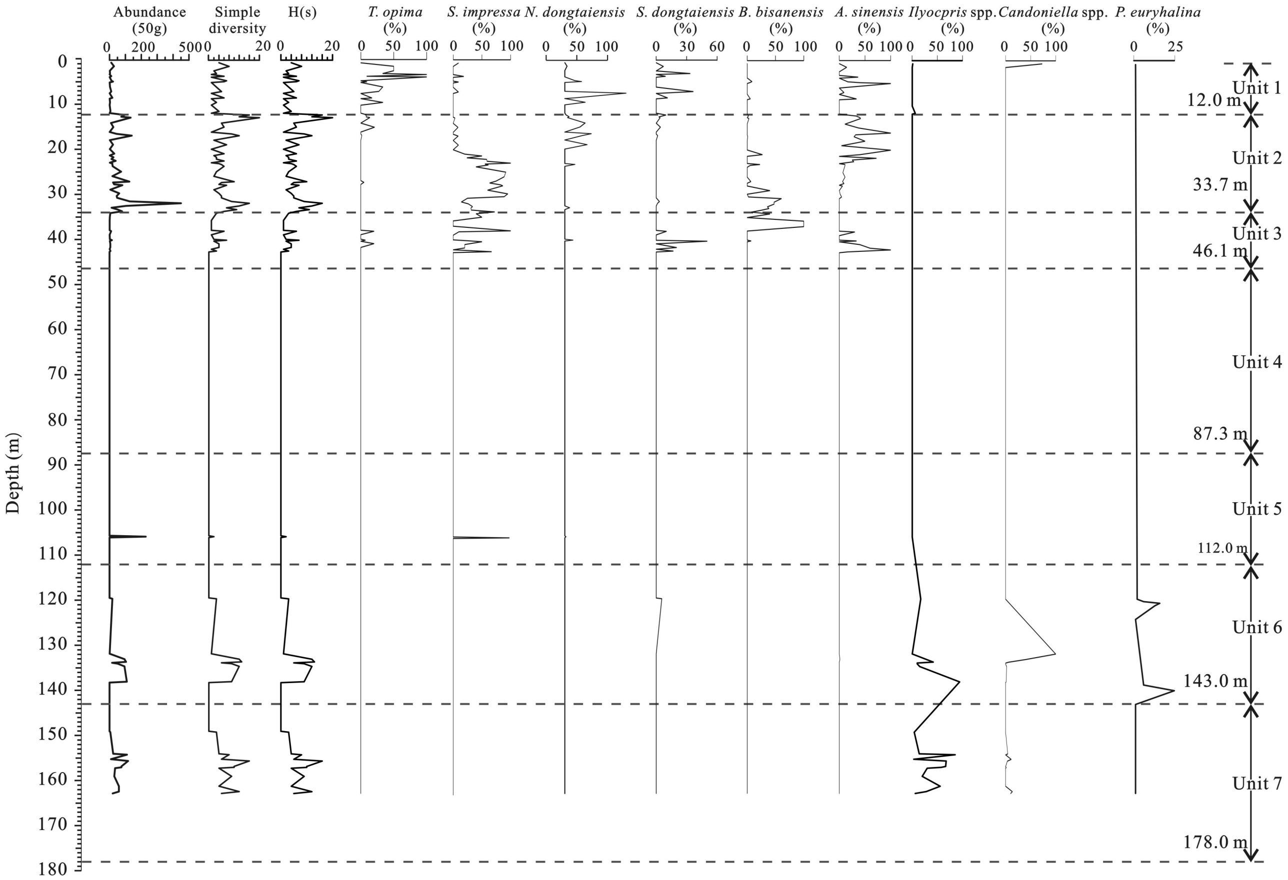

Fig. 4. Downcore changes in ostracod abundance, simple diversity, and Shannon index (H(s)), and the relative abundance of the main ostracod species in the uppermost 180 m of core LZK1.

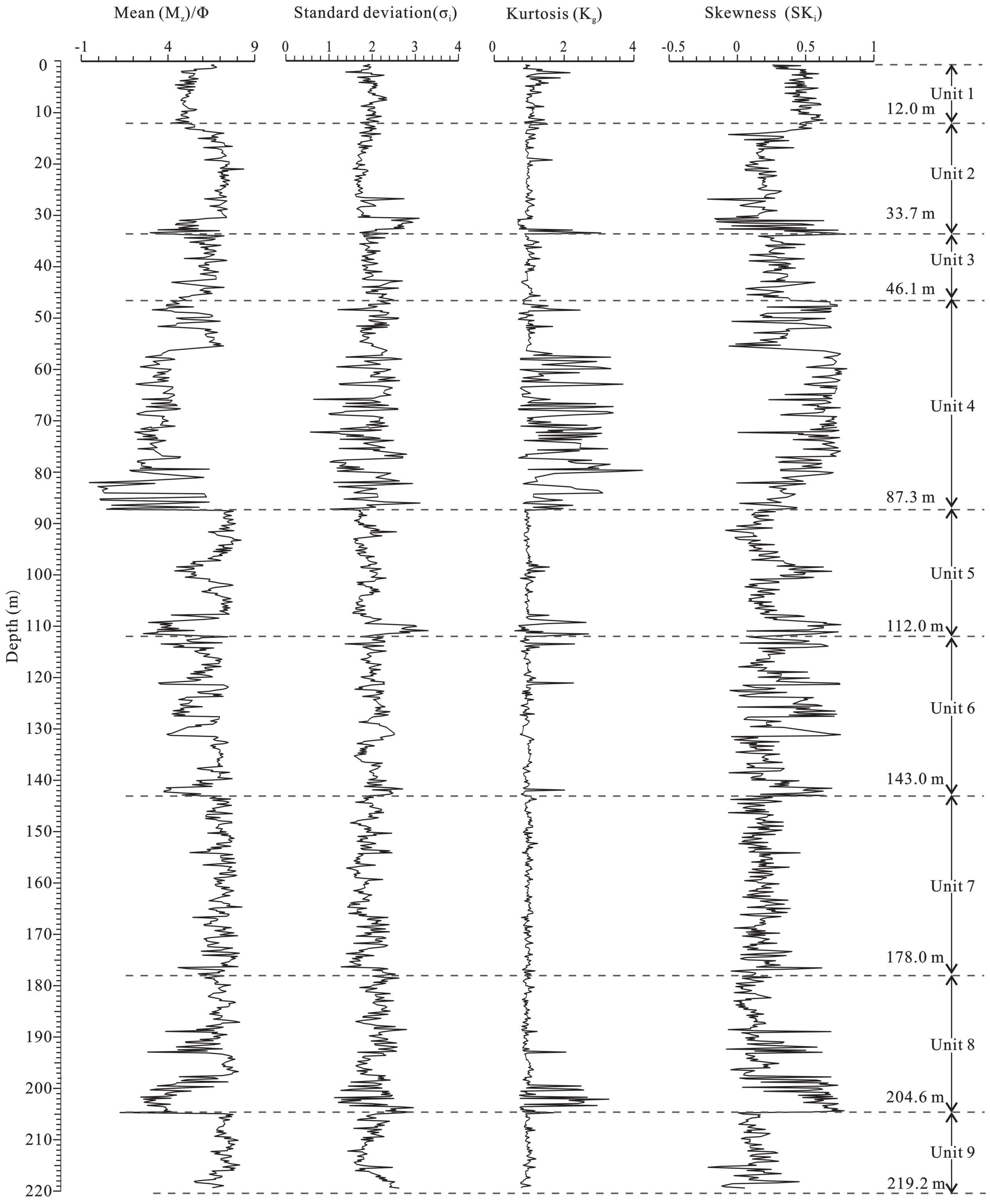

Fig. 5. Downcore changes of grain-size parameters: mean (M_z), standard deviation (σ_i), kurtosis (K_g), skewness (SK_i).

dramatically since the Quaternary. The value of σ_i extends from 0.56–3.3 and mostly concentrates within a narrow range from 1.5 to 2.5. In general, the trend of σ_i indicates the variation of sorting. The considerably broad range of σ_i suggests that the sorting is poor. SK_i and K_g indicate the genesis of sediments as reflected in the normality of their size distributions (Folk, 1966). Most of the LZK1 samples are positively skewed, which implies that the sediments mainly consist of coarse grains. The value of K_g varies from 0.58 to 4.25 (mostly concentrated in a narrow band from 0.4 to 0.8), indicating that most of the normal curves are platykurtic distributions.

5 Discussion

5.1 Quaternary chronostratigraphic framework

By using the magnetostratigraphic results (Fig. 2) together with the OSL and AMS ^{14}C dates (Tables 1 and 2), we were able to establish a chronostratigraphic framework for the sedimentary sequence of core LZK1. Two geomagnetic boundaries were recorded in the core over the depth range 0.6–219.2 m: the Matuyam/Gauss (M/Ga) chron boundary at 219.2 m and the Brunhes/Matuyama (B/M) chron boundary at 143.0 m (Fig. 2). The Ga/M boundary is dated to 2.58 Ma (Ogg, 2012), which is the basal age of the Quaternary. The B/M boundary has been dated to 0.781 Ma (Hilgen et al., 2012), which is the age boundary between the Middle Pleistocene and Calabrian. Therefore, Units 7, 8, and 9 were deposited from 2.58 Ma to 0.78 Ma, in the Calabrian and Gelasian.

As defined above, we interpret Unit 6 (112.0 to 143.0 m) to have been deposited from 780 Ka to 126 Ka in the Middle Pleistocene, according to the Upper/Middle Pleistocene boundary and the B/M boundary. The Upper/Middle Pleistocene boundary of core LZK1 can be correlated with the boundary of the cores in the southern bank of the Yangtze distributary (Chen et al., 1997; Wang et al., 2005) and Chongming Island (Li, 2005).

In Unit 5 (87.3 to 112.0 m), the magnetic reversal at 106.2 m can be correlated with the Blake Magnetic Excursion (120 Ka) (Fig. 2). Additionally, the OSL sample at 107.1 m (age of 124.5 Ka on average) is about 5 m above the boundary (112 m) between Unit 5 and Unit 6. Moreover, the core section from 108.0 to 112.0 m consists of medium-fine sand with gravels, overlain by clay interbedded with silt upwards. In comparison, the section below 112.0 m consists of interbedded clay and sand, showing a sudden depositional change around 112.0 m (Fig. 3a). Thus, we infer the depth of the Upper/Middle Pleistocene boundary to be 112.0 m. Therefore, Unit 5 was formed from 126 Ka to 95 Ka in the early Upper Pleistocene, based on the OSL date at core depth 87.5 m.

As described above, in Unit 4, the core section of 55.2 to 87.3 m includes upward-fining deposits consisting of coarse sand with gravels, medium-fine sand, fine sand, and silt (Fig. 2a). During the Last Glacial Maximum (LGM), a huge incised valley was formed in the present Yangtze delta area (Li et al., 2000). The deeply incised paleo-valley was filled by upward-fining deposits during the post-glacial sea-level rise. (Li et al., 2000, 2002). Therefore, the incised-valley sequence from Unit 4 to Unit 1 was deposited continuously since the LGM. These sedimentary successions can be observed in several cores distributed in the incised Yangtze paleo-valley area (Chen et al., 2000; Hori et al, 2001a, 2002; Xu et al., 2013; Zhao et al., 2017). The OSL dates at the core depths of 87.5 m and 86.8 m are 95.5 Ka and 63.2 Ka, respectively, indicating that a depositional hiatus existed between 87. 5 m and 86.8 m. Since the valley cuts into the Middle to Upper Pleistocene deposits (Chen and Stanley, 1995), the OSL date at the depth of 86.8 suggests that the base of the unit may represent the lag deposits. The OSL dates at the sections of 43.3 m and 57.0 m seem to conflict with the continuous deposits since the LGM. The overestimated ages from these two samples are probably caused by partial bleaching, which frequently occurred in the coastal/shelf environment (Wang et al., 2015). Thus, it can be concluded that Unit 4 was deposited from after the LGM to the end of the Upper Pleistocene.

From the OSL dating results at 41.6 m (11.1 ± 0.5 ka.), it can be inferred that the magnetic reversal at 41.0 m correlates to the Gothenburg Magnetic Excursion (12–13 Ka BP), (Fig. 2; Mörner, 1977). Furthermore, based on the appearance of large numbers of foraminifera and ostracoda at 46.1 m (Figs. 3 and 4), which indicates a transgression in the Holocene (Wang et al., 1981; Ke et al., 2017), the Holocene deposits can be defined. Thus, it can be concluded that Unit 1 to Unit 3 inclusive were formed in the Holocene.

5.2 Lithostratigraphic subdivision

According to the lithological stratification characteristics and stratigraphic unit division in the Shanghai area, from bottom to top, the Quaternary stratigraphic sequence of core LZK1 can be subdivided into Anting Formation, Jiading Formation, Chuansha Formation, Nanhui Formation, Loutang Formation, Shanghai Formation, and Rudong Formation. The lower Pleistocene Anting Formation includes three members, namely Unit 7, Unit 8 and Unit 9. The Middle Pleistocene Jiading Formation can be correlated with Unit 6. The Upper Pleistocene Chuansha Formation and Nanhui Formation are likely associated with Unit 5 and Unit 4, respectively. The Holocene Loutang Formation, Shanghai Formation, and Rudong Formation correspond to Unit 3, Unit 2 and Unit 1, respectively (Fig. 6).

Table 1 AMS ^{14}C dates of core LZK1

Laboratory No.	Core depth (m)	Material	Conventional age (a BP)	Cal age (2δ, Cal a BP)
Beta-345637	20.6	Shell	3000±30	2760–2690
Beta-345638	21.2	Shell	3110±30	2910–2760
Beta-345639	30.8	Shell	4890±30	5260–5030
Beta-345641	32.8	Shell	6290±30	6760–6630

Table 2 OSL dates of core LZK1

Field No.	Depth(m)	U(ppm)	Th(ppm)	K(%)	Total dose(Gy)	Total dose rate(Gy/Ka)	Water content(%)	Age(Ka)
gsg-1	13.6	1.80	9.80	1.80	4.94±0.37	3.02	27.26	1.6±0.1
gsg-2	14.0	2.56	13.7	2.25	6.50±0.19	3.78	36.92	1.7±0.1
gsg-5	41.6	2.30	12.7	2.26	41.04±0.71	3.71	29.98	11.1±0.5
gsg-6	43.3	1.76	8.70	1.63	43.62±0.31	2.77	22.68	15.6±0.6
gsg-7	57.0	1.54	7.25	1.77	82.56±1.17	2.74	20.39	30.1±1.3
gsg-8	86.8	1.20	5.56	1.82	168.70±2.901	2.67	10.82	63.2±3.4
gsg-9	87.5	2.91	15.5	2.67	435.76±15.62	4.56	27.35	95.5±5.1
gsg-10	107.1	3.11	14.4	2.24	532.54±6.40	4.28	20.57	124.5±5.22

Age (Ka)	Epoch	Unit	Stratigraphy	Depth (m)	Lithology
	Holocene	1	Rudong Formation (Qh_1r)	0.6-13.7	Gray silty clay and silt alternated, with horizontal bedding and microwave bedding.
		2	Shanghai Formation (Qh_1s)	13.7-33.7	Gray clay, intercalated with the thin layer of silt and clayey silt, the silt layer contains shells and shell debris. Lenticular bedding, horizontal bedding, and convolute bedding in some parts.
		3	Loutang Formation (Qh_1l)	33.7-46.1	Lower part: taupe or grayish-yellow silt and silty clay, high organic matter, occasional roots of plants and shell debris, horizontal bedding. Upper part: gray-taupe clay interbeded with silt and clayey silt, with sand lens, horrizontal bedding and convolute bedding
11.7	Upper Pleistocene	4	Nanhui Formation (Qp_3n)	46.1-87.3	Yellowish-gray coarse sand with gravel, medium-fine sand, silty fine sand, the lower part contanis more subangular or subcircular gravels which diameters range from 2 to 5 mm. Grain size shows fining-upward trends, partially with clay and silt, with horizontal bedding, wavy bedding, and flaser bedding.
126		5	Chuansha Formation (Qp_3c)	87.3-112.0	Gray medium-fine sand in the bottom, occasional subangular or subcircular gravels with diameters span from 2-3 mm, overlain by gray plastic clay, with horizontal bedding and wavy bedding.
	Middle Pleistocene	6	Jiading Formation (Qp_2j)	112.0-143.0	Grayish-yellow silty fine sand with parallel bedding, overlain by gray or grayish-yellow silt/clayey silt- clay sedimentary cycles, containing abundant white shell debris,with iron and manganese spots and calcareous concretions, lenticular bedding and horizontal bedding.
781	Calabrian	7	The third member of Anting Formation (Qp_1a^1)	143.0-178.0	Grayish-yellow or blueish-gray clay, with thin layers of clayey silt or silty clay, partially clay interbeded with clayey silt, horizontal bedding.
1800		8	The second member of Anting Formation (Qp_1a^2)	178.0-204.6	Grayish-yellow corse sand and silty fine sand with gravels in the bottom, overlain by 4 slit/silty clay-clay sedimentary cycles, with iron and manganese spots, calcareous bands and concretions.
2580	Gelasian	9	The first member of Anting Formation (Qp_1a^3)	204.6-219.2	Grayish-yellow or blueish-gray silt, silty clay, and clay, containing iron and manganese spots, calcareous bands, and concretions.

Fig. 6. Stratigraphic division and lithology of core LZK1.

5.3 Sedimentary environment and marine transgressions

Units 7, 8, and 9 (143.0 to 219.2 m) include several upward-fining depositional cycles consisting of lower sandy beds and upper muddy beds (Fig. 2). The M_z value in Unit 9 is the highest among all depositional units of the core (Fig. 5). In general, the σ_i value is relatively low in Unit 9 (Fig. 5), indicating a stable sedimentary environment with weak hydrodynamic force. The base of Unit 8 (204.2–197.6 m) consists of coarse sand with gravels. Thus, the M_z value suddenly drops then rises again. The values of SK_i and K_g show a sudden rise, suggesting the depositional environment has changed at the bottom of Unit 8. Units 8 and 9 are completely devoid of foraminifers and ostracods (Fig. 3 and Fig. 4). In unit 7, the M_z value is extremely high and σ_i value fluctuates slightly. This unit is also devoid of foraminifers but contains a terrestrial ostracod assemblage with relatively low abundances (mostly <100). The ostracod assemblage is composed predominantly of *Ilyocpris* spp., *Candona* spp., *Candoniella* spp. and *Ilyocpris* spp. (Fig. 4), which are widely distributed in fresh to brackish water (e.g., lakes, rivers, and marshes), indicating flowing water or a slow-flowing water environment (Xie et al., 2009). Most species of *Candona* and *Candoniella* are fresh-water genera (Luo et al., 2010). Therefore, Unit 7 to Unit 9 are interpreted as freshwater lacustrine deposits. The lower part of these three units, which contains more sandy beds, may change from shallow lake to shore lake. The abundant iron and manganese spots and calcareous concretions in the muddy beds of the lower part suggest subaerial exposure and pedogenic modification. The water depth increased in the upper part of these three units, with more muddy beds.

Unit 6 (112.0 to 143.0 m) contains several upward-fining depositional cycles consisting of lower sandy beds and upper muddy beds, with an alternation of silt and clay in the middle and upper parts of the unit (Fig. 2 and Fig. 5). Shell fragments are common and an ostracod assemblage of terrestrial (e.g., *Ilyocpris* spp.) and euryhaline marine species (e.g., *Sinocythere dongtaiensis*) can be identified (Fig. 4). In general, the value of M_z increased compared with Unit 7. M_z and SK_i values fluctuate severely (Fig. 5). These features indicate that the hydrodynamic force increased. The supply source may have changed. The iron and manganese spots and calcareous concretions observed in the unit also indicate subaerial exposure. Accordingly, Unit 6 is interpreted as an alternation of lakeshore and shallow lake environment. The lake was subject to marine influenced when the marine ostracods appeared. Since the unit was interpreted as being deposited in the Middle Pleistocene, it may have been affected by the 'Jiading marine transgression' (Qiu and Li, 2007).

Unit 5 (87.3 to 112.0 m) consists of medium-fine sand with gravel in the basement, and clay intercalated upward with a thin layer of silt (Fig. 2). The M_z value shows an upward-increasing- trend, suggesting a fining trend in the sediments. The σ_i value decreased (Fig. 5), which means that the hydrodynamic force weakened. In this unit, the ostracod assemblage has a relatively high abundance but a simple diversity (only two species) (Fig. 4), the dominant species being *Sinocytheridea impressa*, which lives in littoral and nearshore environments (Li et al., 2015). The foraminiferal assemblage in this unit has the highest abundance among all depositional units of the core, with simple diversities (between 2 and 6) (Fig. 4). The assemblage is dominated by *Ammonia beccarii* vars, which is a euryhaline species. Based on the lithological characteristics and the benthic foraminifera and ostracod assemblages, in conjunction with the depositional period inferred above, the basement of Unit 5 is interpreted as having been deposited in the branch channel of a delta plain environment, which then changed to a lagoonal environment when it experienced a marine transgression in the early Upper Pleistocene (100-80 Ka; Wang et al., 2004).

Unit 4 (46.1 to 87.3 m) is characterized by gradually upward-fining deposits from coarse sand with gravels to silt (Fig. 2). The upper part of this unit consists of an alternation from silt to clayey silt and clay (Fig. 2). The M_z value is the lowest among all depositional units of the core, ascending upward, σ_i, K_g and SK_i values fluctuate severely, which are indicative of a hydrodynamic force increasing strength and instability. This unit is free of foraminifers and ostracods and was deposited in the incised Yangtze paleo-valley, changing from fluvial channel to floodplain environment with rising sea-level (Li et al., 2000, 2002; Hori et al., 2001b, 2017).

Unit 3 (33.7 to 46.1 m) is characterized by alternating clay and silty clay (Fig. 2). The M_z value increased in comparison to Unit 4, reflecting a weakening hydrodynamic force. In this unit, both the foraminifers and the ostracods are in low abundance (Fig. 3 and Fig. 4), the foraminifer assemblage being dominated by *Ammonia beccarii* var. and *Florilus decorus* (Ke et al. 2017), which are euryhaline species. The ostracod assemblage is dominated by littoral and nearshore species: *Sinocytheridea impressa*, *Bicornucythere bisanensis* and *Pistcythereis bradyformis*. Based on the lithological characteristics and benthic foraminifer and ostracod assemblages, Unit 3 is interpreted as having been deposited in a delta front, representing the beginning of the marine transgression in the early Holocene (Chen et al., 2003; Xu et al., 2016).

Unit 2 (12.0 to 33.7 m) consists of clay, intercalated with silty clay and silt (Fig. 2). The M_z value increased and σ_i decreased compared with Unit 3 (Fig. 5), showing a weak hydrodynamic force and better sorting of the sediments. In this unit, the benthic foraminiferal assemblage has a moderately high abundance and diversity (Fig. 3). The assemblage is dominated by *Ammonia beccarii* var. and *Elphidium advenum* (Ke et al., 2017). The ostracod assemblage has the highest abundance among all depositional units of the core with a moderately high diversity (Fig. 4). The assemblage is dominated by *Neomonoceratina dongtaiensis*, *Albileberis sinesis*, *Bicornucythere bisanensis* and *Sinocytheridea impressa*. Some deep-water species such as *Trachyleberis scabrocuneata*, *Munseyella Japonilca*, *Munseyella pupilla*, and *Aurila cymba* are relatively abundant. Thus, Unit 2 is interpreted as deposits of a prodelta or shallow sea environment, suggesting the strongest transgression during the middle Holocene.

Unit 1 (0.6 to 12.0 m) is characterized by alternation of clayey silt and silt (Fig. 2). The M_z value decreased and the SK_i value increased significantly compared to Unit 2. In general, the value of σ_i shows an upward-ascending trend (Fig. 5). The variation of these values indicates that the hydrodynamic force changed during this period. In this unit, both foraminifers and ostracods are in relatively low abundance (Figs. 3 and 4). The foraminiferal assemblage is dominated by *Ammonia beccarii* var. and *Florilus decorus*. The ostracod assemblage is dominated by brackish water and euryhaline species (*Tanella opima, Neomonoceratina dongtaiensis, and Albileberis sinesis*). The terrestrial species appear in the 0.6 to 1.5 m core section. Accordingly, Unit 1 was deposited in a delta front environment when the marine regression happened in the late Holocene. Unit 1 to Unit 3 can be correlated with the '*Ammonia* marine transgression' during the Holocene (Wang et al., 1981; Ke et al., 2017).

6 Conclusions

This study provided a chronostratigraphic framework for studying the stratigraphic correlation in the Yangtze incised paleo-valley since the start of the Quaternary, based on an integrated analysis of lithological characteristics of the core with dates from magnetostratigraphic, AMS^{14}C and OSL, and microfossils (benthic foraminifers and ostracods). The following conclusions can be drawn:

(1) The boundaries between the Holocene and Pleistocene, between the Upper Pleistocene and Middle Pleistocene, and between the Middle Pleistocene and the Calabrian, are estimated to be at ~46.1 m, ~112.0 m, and ~143.0 m of the core section, respectively.

(2) From the bottom upwards, the Quaternary stratigraphic sequence of core LZK1 can be subdivided into the lower Pleistocene Anting Formation, Middle Pleistocene Jiading Formation, Upper Pleistocene Chuansha Formation and Nanhui Formation, Holocene Loutang Formation, Shanghai Formation, and Rudong Formation.

(3) Three marine transgressions can be identified since the beginning of the Quaternary, which can be correlated to the Middle Pleistocene 'Jiading marine transgression', the early Upper Pleistocene marine transgression and the Holocene '*Ammonia* marine transgression'.

(4) The sedimentary environments of the Hengsha Island area can be interpreted as a freshwater lacustrine environment during the early Pleistocene, an alternation between shallow lake and lakeshore environment during the Middle Pleistocene, a delta plain to lagoonal environment during the early Upper Pleistocene, a fluvial channel to floodplain environment from the LGM to the end of the Upper Pleistocene, and a deltaic environment during the Holocene.

Acknowledgments

We thank two anonymous reviewers for their detailed and constructive reviews, which considerably improved the manuscript. This research is funded by the Geological Survey of China (Nos. DD20190370, DD20160345-07) and the National Natural Science Foundation (No. 40902049).

Manuscript received Apr. 5, 2020
accepted Jun. 5, 2020
associate EIC: DING Xiaozhong
edited by Jeff LISTON and FEI Hongcai

References

Chen, Z.Y., Chen, Z.L., and Wang, Z.H., 1997. Quaternary stratigraphy and trace-element indices of the Yangtze delta, Eastern China, with special reference to marine transgression, Quaternary Research, 47(2): 181–191.

Chen, Z.Y., Song, B.P., Wang, Z.H., and Cai, Y.L., 2000. Late Quaternary evolution of the subaqueous Yangtze Delta, China: sedimentation, stratigraphy, palynology, and deformation. Marine Geology, 162: 423–441.

Chen, Z.Y., and Stanley, D., 1995. Quaternary subsidence and river channel migration in the Yangtze Delta plain, Eastern China, Journal of Coastal Research, 11(3): 927–945.

Chen, Z.Y., Saito, Y., Hori, K., Zhao, Y.W., and Kitamura, A., 2003. Early Holocene mud-ridge formation in the Yangtze offshore, China: a tidal-controlled estuarine pattern and sea-level implication. Marine Geology, 198: 245–257.

Cheng, Y., Li, X.Q., Shu, J.W., Bai, S.B., Zhao, Z.Y., Zhang, X.Y., Guo, G., Zhang, P., and Lin, J.X., 2019. Sedimentary Evolution and Transgressions of the Western Subei Basin in Eastern China since the Late Pliocene. Acta Geologica Sinica (English Edition), 93(1): 155–166.

Duan, Z.Q., Liu, Q.S., Shi, X.F., Yao, Z.Q., Liu, J.X., and Su, K., 2016. Reconstruction of high-resolution magnetostratigraphy of the Changjiang (Yangtze) River Delta, China. Geophysical Journal International, 204: 948–960.

Folk, R.L., 1966. A review of grain-size parameters. Sedimentology, 6: 73–93.

Folk, R.L., and Ward, W.C., 1957. A Study in Significance of Grain Size Parameters. Journal of Sedimentary Petrology, 27: 3–26.

Guo, Y.G., Li, Y.C., Xu, D.Y., Li, X.Q., and Zhang, X.H., 1997. Tectonic evolution of Yellow Sea and East China Sea continental shelf and adjacent areas. Marine Geology and Quaternary Geology, 17: 1–11 (in Chinese with English abstract).

Han, D., and Yu, H., 2001. Relationship of activity of the Eastern Asia Monsoon in late stage of Upper Pleistocene and the sedimentary environment. Journal of the Ocean University of Qingdao, 31(6): 911–916 (in Chinese with English abstract).

Hilgen, F.J., Lourens, L.J., and Van Dam, J.A., 2012. The Neogene Period. In: Gradstein, F.M., Ogg, J.G., Schmitz, M.D., and Ogg, G.M. (eds.), The Geological Time Scale. Amsterdam: Elsevier, 923–978.

Hori, K., and Saito, Y., 2017. Differences in radiocarbon ages among molluscan shells, plant materials, and total organic carbons: An example from the paleo-Changjiang incised-valley fill, China. Quaternary International, 455: 45–55.

Hori, K., Saito, Y., Zhao, Q.H., Cheng, X.R., Wang, P.X., Sato, Y., and Li, C.X., 2001a. Sedimentary facies of the tide-dominated paleo-Changjiang (Yangtze) estuary during the last transgression. Marine Geology, 177: 331–351.

Hori, K., Saito, Y., Zhao, Q.H., Chen, X.R., Wang, P.X., Sato, Y., and Li, C.X., 2001b. Sedimentary facies and Holocene progradation rates of the Changjiang (Yangtze) delta, China. Geomorphology, 41: 233–248.

Hori, K., Saito, Y., Zhao, Q.H., and Wang, P.X., 2002. Control of incised-valley fill stacking patterns by accelerated and decelerated sea-level rise: the Changjiang example during the last deglaciation. Geo–Marine Letters, 22: 127–132.

Huang, W.S., Chen, H.P., Xu, F., Meng, Z., Zhang, F.Q., and Wu, S.W., 2019. Gradual Evolution from Fluvial Dominated to Tide Dominated Deltas and Channel Type Transformation: A Case Study of MPE3 Block in the Orinoco Heavy Oil Belt of the Eastern Venezuelan Basin. Acta Geologica Sinica (English Edition), 93(6): 1909–1921.

Jiang, L.Z., Zhang, Y.L., Wang, K.F., Zhang, W.D., and Zhang, M.B., 2000. Palynological assemblages of Pleistocene from Shanghai Region and its palaeovegetation and palaeoclimate. Shanghai Geology, 76: 34–41 (in Chinese with English abstract).

Ke, X., Li, B.H., Zhang, Z.Y., Wei, Y., Hu, F., Fan, D.W., Sun, L., Xie, J.L., Yu, J.J., and Yao, H.Z., 2017. Post-glacial Foraminifera of the incised Yangtze paleo-valley and paleoenvironmental implications. Journal of Paleontology, 9 (16): 1102–1122.

Li, C.X., Chen, Q.Q., Zhang, J.Q., Yang, S.Y., and Fan, D.D., 2000. Stratigraphy and paleoenvironmental changes in the Yangtze Delta during the Late Quaternary. Journal of Asian Earth Sciences, 18: 453–469.

Li, C.X., Wang, P., Sun, H.P., Zhang, J.Q., Fan, D.D., and Deng, B., 2002. Late Quaternary incised-valley fill of the Yangtze delta (China): its stratigraphic framework and evolution. Sedimentary Geology, 152: 133–158.

Liu, J., Saito, Y., Kong, X.H., Wang, H., Xiang, L.H., Wen, C., and Nakashima, R., 2010. Sedimentary record of environmental evolution off the Yangtze River estuary, East China Sea, during the last ~13,000 years, with special reference to the influence of the Yellow River on the Yangtze River delta during the last 600 years. Quaternary Science Reviews, 29: 2424–2438.

Li, X.Y., Zhao, Q.H., Yao, Z.Q., Wang, Q., Jian, Z.M., and Shi, X.F., 2015. Transgressive records of last million years in the Bohai area, China: evidence from foraminifera and ostracoda of Core BH08. Marine Geology & Quaternary Geology, 35(6): 93–108 (in Chinese with English abstract).

Li, Z.Y., 2005. Strata of Quaternary and Evolution of Sedimentary Environment in Yangtze Estuary (MSc thesis). Shanghai: East China Normal University, 1–86 (in Chinese with English abstract).

Luo, M.S., Lv, X.L., Zhang, K X., Chen, F.N., Xu, Y.D., Chen, R.M., and Song, B.W., 2010. Middle Miocene-early Pliocene ostracod assemblages in the Xunhua Basin, Qinghai and their geological significance. Acta Micropalaeontologica Sinica, 27 (2): 125–134 (in Chinese with English abstract).

Mörner, N.A., 1977. The Gothenburg magnetic excursion. Quaternary Research, 7(3): 413–427.

Ogg, J.G., and Smith, A.G., 2012. Chapter 5 – Geomagnetic Polarity Time Scale. In: Felix, M.G., Ogg, J.G., Schmitz, M.D., and Ogg, G.M. (eds.), The Geologic Time Scale. Amsterdam: Elsevier, 85–113.

Qiu, J.B., 2006. The Progress of Quaternary geologic study in Shanghai. Shanghai Geology, 4: 5–9 (in Chinese with English abstract).

Qiu, J.B., and Li, X., 2007. Quaternary strata and sedimentary environment in Shanghai. Shanghai: Shanghai Science &Technology Press, 1–225 (in Chinese).

Shannon, C.E., 1948. A mathematical theory of communication: The Bell System Technical Journal, 27: 379–423, 623–656.

Singer, B.S., 2014. A Quaternary geomagnetic instability time scale. Quaternary Geochronology, 21: 29–52.

Wang, P.X., Min, Q.B., Bian, Y.H., and Chen, X.R., 1981, Strata of Quaternary transgressions in East China: Acta Geologica Sinica, 1: 1–13 (in Chinese with English abstract).

Wang, Y., Long, H., Yi, L., Yang, L.H., Ye, X.Y., and Shen, J., 2015. OSL chronology of a sedimentary sequence from the inner-shelf of the East China Sea and its implications for post-glacial deposition history. Quaternary Geochronology, 30: 282 –287.

Wang, Z.H., Li, M.T., Zhang, R.H., Zhuang, C.C., Liu, Y., Saito, Y., Xie, J.L., and Zhao, B.C., 2011. Impacts of human activity on the late Holocene development of the subaqueous Yangtze delta, China, as shown by magnetic properties and sediment accumulation rates. The Holocene, 21: 393–408.

Wang, Z.H., Qiu, J.B., Ran, L.H., Yan, X.X., and Li, X., 2004. Chronostratigraphy and transgression/regression during late Pleistocene in the southern Changjiang (Yangtze) river delta plain. Marine Geology & Quaternary Geology, 24 (4): 1–8.
Wang, Z.H., Xu, H., Zhan, Q., Saito, Y., He, Z.F., Xie, J.L., Li, C.X., and Dong, Y.H., 2010. Lithological and palynological evidence of late Quaternary depositional environments in the subaqueous Yangtze delta, China. Quaternary Research, 73: 550–562.
Wang, Z.H., Zhang, D., Li, X., Tao, S.K., and Xie, Y., 2008. Magnetic properties and relevant minerals of late Cenozoic sediments in the Yangtze River delta and their implication. Geology in China, 35: 670–682. (in Chinese with English abstract).
Wang, Z.J., Chen, Z.Y., Wei, Z.X., Wang, Z.H., and Wei, T.Y., 2005. Coupling controls of neotectonism and paleoclimate on the Quaternary sediments of the Yangtze (Changjiang) coast. Chinese Science Bulletin, 50(16): 1775–1784.
Wu, B.Y., and Li, C.X., 1987. Quaternary Geology of Yangtze Delta. Beijing: China Ocean Press, 1–170 (in Chinese).
Xie, J.L., Zhang, K.X., Ma, X.L., Zhao, B.C., and Zhang, P., 2017. Magnetostratigraphy and Astronomically Tuned Time Scale of Yangtze Delta since Pliocene. Earth Science, 42(10): 1761–1771 (in Chinese with English abstract).
Xie, J.L., 2017. Sedimentary response research of major climate trasition events since Pliocene, Changjiang Delta (Ph.D. thesis). Wuhan: China University of Geosciences (Wuhan), 1–133 (in Chinese with English abstract).
Xie, M.P., Zhu, L.P., Peng, P., Wang, J.B., Wang, Y., and Schwalb, A., 2009. Ostracod assemblages and their environmental significance from the lake core of the Nam Co on the Tibetan Plateau 8.4 Ka BP. Journal of Geographical Sciences, 19: 387–402.
Xu, T.Y., Shi, X.F., Wang, G.Q., Qiao, S.Q., Yang, G., Liu, S.F., Wang, X.C., and Zhao, Q.H., 2013. Sedimentary facies of the subaqueous Changjiang River delta since the late Pleistocene. Chinese Journal of Oceanology and Limnology, 31: 1107–1119.
Xu, T.Y., Wang, X.C., Wang, G.Q., Wang, X., Shi, X.F., Yao, Z.Q., Yang, G., Fang, X.S., Qiao, S.Q., Liu, S.F., and Zhao, Q., 2016. Sequence stratigraphy of the subaqueous Changjiang (Yangtze River) delta since the Last Glacial Maximum. Sedimentary Geology, 331: 132–147.
Zhang, X., Dalrymple, R.W., and Lin, C.M., 2017. Facies and stratigraphic architecture of the late Pleistocene to early Holocene tide-dominated paleo–Changjiang (Yangtze River) delta. The Geological Society of America Bulletin, 130: 455–483.
Zhao, B.C., Yan, X.X., Wang, Z.H., Shi, Y.J., Chen, Z.Y., Xie, J.L., Chen, J., He, Z.F., Zhan, Q., and Li, X., 2018. Sedimentary evolution of the Yangtze River mouth (East China Sea) over the past 19,000 years, with emphasis on the Holocene variations in coastal currents. Palaeogeography, Palaeoclimatology, Palaeoecology, 490: 431–449.

About the first and corresponding author

KE Xue, female, born in 1984 in Huangshan City, Anhui Province; Doctor; graduated from China University of Geosciences (Wuhan); research assistant at the Institute of Geological Survey, China University of Geosciences (Wuhan). She is interested in the study of Quaternary deposits in coastal areas and paleoenvironmental reconstruction. Email: xue_ke@cug.edu.cn; phone: 17771431917.